

# Ground-based exploration of the outer Solar system by serendipitous stellar occultations<sup>★</sup>

A. Doressoundiram,<sup>1†</sup> F. Roques,<sup>1</sup> Y. Boissel,<sup>2</sup> F. Arenou,<sup>2</sup> V. Dhillon,<sup>3</sup> Stu Littlefair<sup>3</sup> and T. Marsh<sup>4</sup>

<sup>1</sup>LESIA, Observatoire de Paris, F-92195 Meudon Principal Cedex, France

<sup>2</sup>GEPI, Observatoire de Paris, F-92195 Meudon Principal Cedex, France

<sup>3</sup>Department of Physics and Astronomy, University of Sheffield, Sheffield S3 7RH

<sup>4</sup>Department of Physics, University of Warwick, Coventry CV4 7AL

Accepted 2012 October 16. Received 2012 October 15; in original form 2012 August 17

## ABSTRACT

Serendipitous stellar occultation technique provides a powerful and unique tool to probe the outer Solar system matter, e.g. Kuiper disc and Oort cloud. We present the results of a serendipitous occultation observation campaign carried out with ULTRACAM, mounted on the ESO-VLT telescope, during 2005 May 17–20. The data are processed using the variability index (VI) method modified. The two-colour data set and the VI method allow searching for occulting objects in term of their distance (50, 200 and 5000 au). The analysis of  $\sim 34$  star-hours provide a working data set for assessing an instrumental approach to search for occultation events by trans-Neptunian objects. We performed recovery tests by implanting synthetic profiles in the data and defining the size of detectable objects to achieve a detection rate of 100 per cent. We propose a Fast Multi-Object Photometer (F-MOP) mounted on a 8-m class telescope and examine its performances. Such instrumental approach from the ground is able to exploit the occultation method for the exploration of the trans-Neptunian region, with a high efficiency.

**Key words:** Kuiper belt: general.

## 1 INTRODUCTION

The trans-Neptunian objects (TNOs) are the frozen leftovers from the formation period of the outer Solar system (Morbidelli, Levi-son & Gomez 2008). The current total mass in the Kuiper belt is estimated to be around 0.03–0.3 Earth masses (Trujillo et al. 2001; Bernstein et al. 2004; Petit et al. 2008), but there is evidence that a much larger mass (10–40  $M_{\text{Earth}}$ ) was originally present at the time of formation (Kenyon & Luu 1998; Schlichting & Sari 2011).

The direct observation of the TNOs does not constrain two important pieces of information: the population of small objects and the outer part of the disc. However, by extrapolation of the density of matter in the Solar system, one might expect that the distribution of sizes (throughout the paper, if not specified, size will be referring to the radius of objects) extends to objects of size much smaller than 1 km and that the Kuiper belt extends beyond 50 au. In addition, estimates for the TNO population calculated from the one event re-

ported by Schlichting et al. (2009) find that 1-km-sized Kuiper belt objects (TNOs) are numerous enough to supply the Jupiter family comets. Further upper limits from Bianco et al. (2009) also find upper limits for a TNO population that is consistent with the scattered disc being the source for the Jupiter family comets.

A very powerful technique to detect tiny and invisible objects by the direct method is to look for their transit in front of a star, which is the serendipitous stellar occultation method (Roques, Georgesvits & Doressoundiram 2008, and references therein). Stellar occultation can detect subkilometre objects beyond the orbit of Neptune. This is applicable provided that the density of the objects is sufficient to cause a significant number of events. Due to their motion on the sky, Solar system objects may pass in front of a star and occult it. If the projected stellar diameter is small enough, the resolution is limited by the so-called Fresnel scale,  $F_s = \sqrt{\lambda D/2}$ , where  $\lambda$  is the observation wavelength and  $D$  is the distance of the TNO, so that  $F_s \sim 1.3$  km typically for  $D = 50$  au and  $\lambda = 480$  nm. Therefore, the light curve of the star will be a diffraction pattern, rather than a simple extinction of flux (Roques & Moncuquet 2000; Nihei et al. 2007).

Serendipitous occultations have no other competing methods, as the magnitudes of the corresponding objects,  $V \sim 35$  or fainter, are unreachable through classical ground-based imaging (Roques et al.

<sup>★</sup>Based on observations obtained at the VLT Observatory Cerro Paranal of European Southern Observatory, ESO, in Chile within the framework of programme 076.C-0436.

<sup>†</sup>E-mail: alain.doressoundiram@obspm.fr

2008). Such occultations can reveal the vertical and radial distribution of the TNOs as far as 50 au and beyond. Also, they provide information on the size distribution down to hectometre-sized objects. This is a key parameter for better understanding formation processes in this remote region of the Solar system. In particular, the primordial structure of the protoplanetary disc just outside the giant planet region has been deeply modified by planetary migrations, resonance trapping and collisions (Farinella, Davis & Stern 2000; Malhotra, Duncan & Levison 2000; Morbidelli et al. 2008). A better knowledge of the Kuiper belt will allow comparisons with circumstellar material around other stars, and provides some clues on the comet belt observed around the  $\beta$ -Pictoris system, and rings or disc-like features akin to Kuiper belts around other young stars.

Fraser et al. (2008) performed a ground-based survey for TNOs, with a limiting magnitude of  $\approx 26.4$ . They found a differential size distribution of TNOs with a slope of  $4.25 \pm 0.25$  for objects with diameter larger than 50 km. This result is consistent with other surveys. Bernstein et al. (2004) with a *Hubble Space Telescope* (*HST*) survey (down to  $m = 29$ ) and Fuentes, George & Holman (2009) with a Subaru pencil beam search (down to  $m = 27$ ) suspect a break in the slope of the size distribution for objects smaller than 40–90 km. Note that the slope for the small objects is not very well constrained.

In Roques et al. (2006, henceforth R06) we reported no detections in the classical Kuiper belt (30–50 au) and the detection of potential hectometre-sized TNOs at a few hundred astronomical units using the 4.2-m William Herschel Telescope. This result brought strong constraints on the low end of the size distribution of the KBOs. A potential TNO of 500 m radius at 45 au has been detected in the *HST* archive data (Schlichting et al. 2009). From a data set of 220 star-hours at a signal-to-noise ratio ( $S/N$ ) of 25 or greater, Bianco et al. (2009) put constraints on 350–500 m radius TNOs.

Several instrumental concepts have been tried to exploit the serendipitous occultation method, playing on the number of targets versus the quality of the data. Good-quality data increase the occultation rate because of smaller/more numerous potential occultors. On the other side, large number of targets increases the observation duration but decreases the occultation rate because detectable objects are larger/less numerous. Observations from space as proposed by Nihei et al. (2007) are the most promising technique. Bickerton et al. (2008) evaluate occultation rate for several configurations.

This paper proposed a new ground-based instrumental concept to exploit the serendipitous occultation method. The serendipitous method needs very good quality light curves to be sure that the observed events are real occultation events and not atmospheric artefacts. Light curves of small angular size target stars allow us to detect the diffraction structure of the profiles which insures the reality of observed occultation events. Stars with small angular size but bright enough to provide a high- $S/N$  light curves are quite rare and need a selection of targets in a large field. An instrument which could monitor enough small bright stars with a large telescope would insure an occultation rate large enough for conducting fruitful statistical study of the Kuiper belt. It could also explore the Oort cloud population. The results expected with such an instrumental concept are estimated from a data set obtained with the ESO-Very Large Telescope (VLT) 8.2-m telescope equipped with the ultrafast camera ULTRACAM. In Section 2, the light curves derived from these data are described, in particular the characteristics impacting the research of occultation events, i.e. signal stability, star size, false positive event and size of detectable objects. In Section 3, these results are used to estimate the performances expected with

such instrumental configuration and the instrumental concept is described in Section 4.

## 2 OBSERVATION WITH THE VLT-ULTRACAM

### 2.1 Observations

We conducted a survey for serendipitous occultations in 2005 May 17–20 using the high-speed, triple-beam imaging photometer ULTRACAM (Dhillon et al. 2007), mounted at the visitor focus of the 8.2-m VLT in Chile. The resulting plate scale on ULTRACAM's three CCD detectors is  $0.15 \text{ arcsec pixel}^{-1}$ , imaging a field of  $2.6 \text{ arcmin}$ . The two stars were observed with frame rates between 61 and 65 Hz, with  $0.002 \text{ s}$  of dead time between exposures. We observed two fields on the ecliptic, each containing two stars of approximately equal brightness, selected from the *Tycho-2* catalogue (Høg et al. 2000) (Table 1). A total of  $\sim 4.0$  million frames were obtained simultaneously in  $g'$  ( $0.48 \mu\text{m}$ ),  $r'$  ( $0.63 \mu\text{m}$ ) and  $u'$  ( $0.35 \mu\text{m}$ ) (Sloan Digital Sky Survey filters; Fukugita et al. 1996).

Data reduction was carried out using the ULTRACAM pipeline data reduction software. After debiasing and flat-fielding the images, source fluxes were extracted by summing the counts in a circular aperture centred on each target star and subtracting a corresponding sky value determined from the (clipped) mean level in an annulus surrounding the star. Stellar fluxes were extracted using variable apertures where the aperture radius was a constant multiple of the seeing, as determined by Moffat fits to the stellar profile. The exact ratio of aperture size to seeing was chosen by reducing the data with a range of values, and selecting the value which minimized the rms variability in the relative light curves of the two target stars. This has the dual effect of optimizing the  $S/N$  and minimizing systematic effects.

The reduced data consist in the light curves for the two stars of the two fields totalling nearly 34 star-hours.

### 2.2 Data quality

An occultation event lasts a tenth of second when observed towards the opposition (Roques & Moncuquet 2000; Nihei et al. 2007). Then, long-term fluctuations of the light curve do not prevent the detection of such brief events. To visualize the temporal variation of the data quality, the  $S/N$  (calculated as the mean value divided by standard deviation value) is computed per sample of 1-min intervals, i.e. one value of  $S/N$  is computed for each 1-min interval (corresponding to 3660 to 3900 points, depending on the frequency of acquisition). The  $S/N$  (1 mn) fluctuates significantly between 10 and more than 200 (Fig. 1, top panel) and the fluctuations have variable time-scales.

The  $S/N$  is also computed on intervals of 1 s (between 61 and 65 points) to test fluctuation of the stellar flux on this time-scale, which is 10 times larger than the typical occultation duration.

The histograms (Fig. 1, middle and bottom panels) of  $S/N$  (1 mn) and  $S/N$  (1 s) indicate that the maximum number of intervals, i.e. longer time, corresponds to  $S/N = 160$ . There are no 1-min interval with  $S/N$  (1 mn) larger than 240, but there are several 1-s intervals with  $S/N$  (1 s) larger than 240. On the other end, there are no interval with  $S/N$  (1 s)  $< 30$  but several tens of minutes where  $S/N$  (1 mn) is smaller than 30. The  $S/N$  (1 s) can be compared with the depth of an occultation event. As computed by Nihei et al. (2009), the depth of an occultation is  $3.\rho^2$ , where  $\rho$  is the occultor radius expressed in Fresnel scale. Considering a detection threshold of eight times the standard dispersion of the light curve (Bickerton

**Table 1** Characteristics of the occulted stars.

	Star	V mag	B - V	Apparent radius at 50 au (m)	Right ascension (J2000)	Declination (J2000)	Ecliptic latitude
Field 1	TYC 6172-150-1	12.47	0.05	550	15:03:25.3	-18:14:42.1	-0°:2
	TYC 6172-155-1	13.33	-0.75	540	15:03:24.1	-18:15:5.9	
Field 2	TYC 6821-1425-1	12.43	-0.27	590	16:50:06.5	-29:40:31.4	-7°:1
	TYC 6821-1317-1	12.29	-0.34	420	16:50:08.6	-29:41:43.6	

The apparent radius has been deduced from the computed spectral class and photometric distance obtained together with extinction from the 2MASS and ULTRACAM Sloan photometry, not the Johnson photometry derived from the *Tycho-2* data.

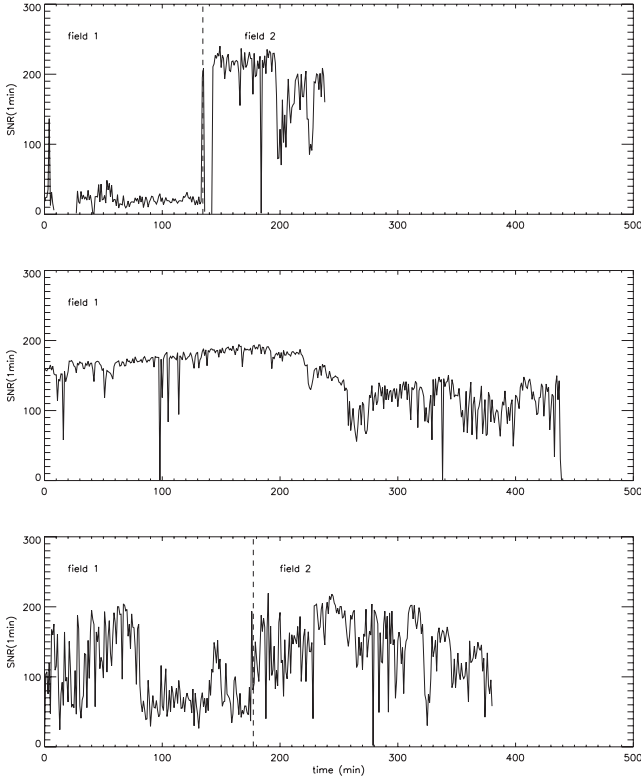


**Figure 1.** Signal-to-noise ratio figures. Top: signal-to-noise ratios for star 1 in each field, for the five runs. The dotted vertical lines separate the nights. This ratio has been derived from 1-min-long intervals of time. Middle: histogram of the S/N for 1-min intervals. Bottom: histogram of the S/N for 1-s intervals.

et al. 2008), an S/N of 240 corresponds to a detectable TNO of 140 m radius. This estimation is confirmed as shown below.

### 2.3 Data analysis

To search for potential occultation profiles, we compute a variability index (VI) measuring the intensity of fluctuations of the light curves, and we search for intervals where VI are deviant from a mean value. Comparison of different wavelength light curves is used to eliminate artefacts as cosmic rays. Comparison of the nearby stars light curves (by computing  $\Delta VI_{\text{int}}$  as explained below) is used to eliminate transparency fluctuations: the remaining deviant intervals are analysed by eyes and, eventually compared with synthetic profiles.

Note that the VI method needs only one hypothesis about event patterns, which is the duration of the expected occultation.

The two-dimensional *variability index*  $VI_{\text{int}}$  is defined as a vector which coordinates are  $[\sigma_{\text{int}}(i, g'), \sigma_{\text{int}}(i, r')]$  and where

$$\sigma_{\text{int}}(i, *) = \sqrt{\frac{1}{N_{\text{int}} - 1} \sum_{j \in \text{int}} \left( \frac{\text{flux}_*(j) - \langle \text{flux}_* \rangle_{\text{int}}}{\langle \text{flux}_* \rangle_{\text{int}}} \right)^2},$$

$i$  is the index of the central point of the interval  $\text{int}$  and  $N_{\text{int}}$  is the number of points of the interval. \* indicates the channel  $g'$  or  $r'$ . We did not use the  $u'$  data for the VI analysis because of the low S/N:

$$\langle \text{flux}_* \rangle_{\text{int}} = \frac{1}{N_{\text{int}}} \sum_{k \in \text{int}} \text{flux}_*(k).$$

This definition of VI is slightly different from the one given in R06. In the latter article, the approach was to interpret the VI distribution as a normal distribution and to search for points deviating more than five times the standard deviation of this distribution. In fact, the VI distribution is different from a normal distribution. Because of scintillation, seeing or absorption, photometric light curves can present large skewness (Roques et al. 2003). The above definition of VI allows analysing fluctuations in the light curves without hypothesis on the VI values distribution. Note that  $VI(i)$  are computed for all points of a light curve. The value of  $\text{int}$  corresponds to the expected duration of the event. The star size is small, then, for an object smaller than one Fresnel scale, the radius of the occultation shadow is  $\sqrt{3} \cdot F_S$  and does not depend on the size of the occulter (Roques & Moncuquet 2000; Nihei et al. 2007). Then, the duration of the occultation, for a null impact parameter, is  $\text{int} = 2 \cdot \sqrt{3} \cdot \frac{F_S}{V_*}$ . It depends on the trajectory of the object through  $V_*$  and, through the value of  $F_S$ , on the occulter distance, but not on its size.  $V_*$  is computed with the hypothesis of a circular orbit in the ecliptic plane. A given distance corresponds to various values of  $\text{int}$ , depending on stars coordinates and dates.  $F_S$  is computed for  $g'$ . For example, the occultation by a small object on a circular orbit at 50 au lasts 0.2 s, or less in the case of a non-zero impact parameter.

We introduce now the vector  $\Delta VI_{\text{int}}$  as the difference  $VI_{\text{int}}(\text{star1}) - VI_{\text{int}}(\text{star2})$ . Its coordinates are as follows:  $[\Delta \sigma_{\text{int}}(i, g'), \Delta \sigma_{\text{int}}(i, r')]$ , where  $\Delta \sigma_{\text{int}} = \sigma_{\text{int}}(\text{star1}) - \sigma_{\text{int}}(\text{star2})$ .

This eliminates the atmospheric events which perturb the two nearby stars in almost the same manner.  $\Delta VI_{\text{int}}$  gives a synthetic representation of the fluctuations of the light curve in a large data set and allow eliminating most of the false events. On the  $\Delta VI_{\text{int}}$  plot, fluctuations affecting *only* star 1 light curve are on the upper right quarter and events of the star 2 light curve are on the lower left quarter. The Fig. 2 represents the  $\Delta VI_{\text{int}}$  with a 150 m radius synthetic object implanted in the light curve of the star 1.

These deviant values of  $\Delta VI_{\text{int}}$  are signature of potential occultation dips. Intervals with deviant  $\Delta VI$  are searched. Points visible in the surrounded region by thick line are the best signature of an occultation of the star 1. Because of the diffraction phenomenon, VI is different in  $g'$  and  $r'$  band. Consequently, the points are not

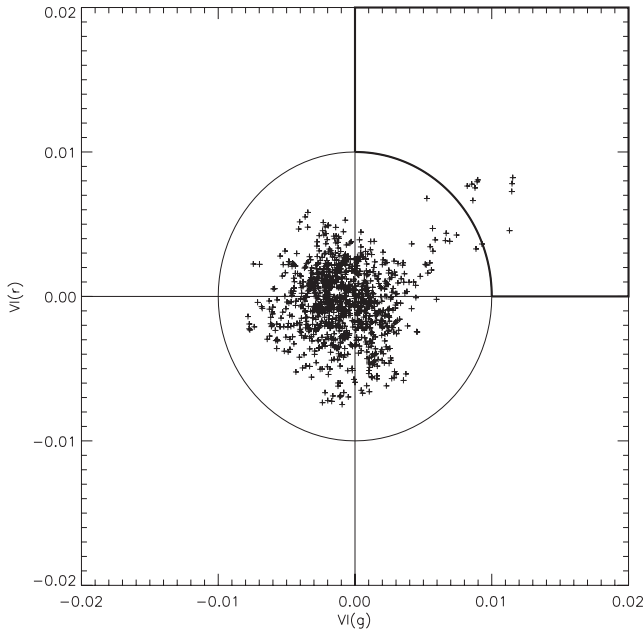


**Figure 2.**  $\Delta V_{\text{int}}$  plot for 0.2-s interval for night 17. The circle indicates the selection criterion, i.e. the  $\Delta VI$  norm equal to 0.01. Any points outside this circle are believed to be the true signature of an occultation event. A synthetic object of 150 m radius at 50 au has been implanted in a 15 s (for clarity purpose) interval of star 1 the light curve. Its signature is clearly visible in the area surrounded by a thick line.

exactly on the diagonal. This is barely visible on Fig. 2 because the  $g'$  and  $r'$  are nearby wavelengths.

The selection criterion is that the  $\Delta VI$  norm, i.e.  $\sqrt{\Delta\sigma_{\text{int}}(i, g')^2 + \Delta\sigma_{\text{int}}(i, r')^2}$ , is larger than 0.01 (circle in Fig. 2). All intervals corresponding to cosmic rays or atmospheric perturbations are eliminated. Tests with synthetic profiles show that values of  $\Delta V_{\text{int}} = 0.01$  corresponds to 150 m radius objects.

The search has been performed on the total of 34 star-hours acquired with ULTRACAM.

To focus the search on the classical Kuiper belt distance, we look for events which duration corresponds to objects at 50 au,  $\text{int} = 0.2$  s. The search leads to four intervals where the norm of  $\Delta V_{\text{int}} > 0.01$ . Three of these intervals correspond to visible absorption artefacts, and the remaining interval is analysed below.

The analysis is also done at 200 au to explore an hypothetical extended Kuiper belt and at 5000 au corresponding to the inner Oort cloud. The  $\text{int}$  values are, respectively, 0.36 s and 1.47 s. The potential event detected at 50 au is also detected at 200 au, and at 5000 au. No other event is detected at 200 au nor at 5000 au.

Two objects of 300 m radius were detected in a 10 h data set by R06, suggesting the existence of an extended cold Kuiper belt.

If the R06 events are signature of real objects, we can cumulate 0 detection with the present data with the R06 data. This gives an estimation of  $10^{13}$  objects, i.e. a fraction of earth mass for a possible extended disc. Analysis of archival *HST* data (Schlichting et al. 2009) has detected no event corresponding to hundred metres objects at 100 au. The reality of such an extended disc is not confirmed. More observations and statistics are needed to confirm this hypothesis.

The potential event occurred in the light curve of the star 1, field 2, during the night 18.

The event affects the star 1, but not the star 2, 79 arcsec away. It lasts 1.1 s and its depth is 7 per cent. It is visible in the three bands

with no difference between the three colours (Fig. 3 b). This event has no diffraction fringes, and *is not* compatible with the occultation by a TNO. However, it is compatible with an occultation by a 4-km object at 1300 au. These parameters are very sensitive to the star's size. The light curve around the event is recomputed from the images with aperture photometry and with different radius ranging from 1.2 to 2.7 arcsec. The event depth, computed with this method, decreases when the aperture radius increases. This shows that the flux drop is due to the spreading of photons outside the aperture and not to decreasing number of photons of the star. We conclude that the event is probably due to seeing conditions and not to an occultation event. This artefact shows that seeing can mimic occultation of one star and not perturb its neighbour star. The fact that the event is 'white', i.e. has no detectable difference in the three colours is an indication of artefact.

This shows that *diffraction signature is the only way to insure the reality of an occultation event*. But it needs the observations to be done in at least two well-separated colours. It needs also that target stars are small enough not to smooth the diffraction profile.

## 2.4 Analysis of the target stars of the VLT observations

We did analysis of the target stars to refine the star size estimation. For this purpose, we made use of the independent infrared Two Micron All Sky Survey (2MASS; Skrutskie et al. 2006) and Denis (Epchtein et al. 1997) survey colours ( $J - H = 0.169$  and  $H - K = 0.078$ ). Those surveys give consistent results indicating a red star instead (K2V, assuming no interstellar extinction). The ULTRACAM Sloan bands ( $u' - g' = 1.470$  and  $g' - r' = 0.350$ ) lead to a solar-type star (F8-G5), compatible with the infrared estimation. The composite colour (the star appearing as blue in visible bands and red in the near-infrared) could be interpreted as the signature of a binary star (red dwarf + white dwarf or hot subdwarf) but this explanation was rejected because of the much too red  $u' - g'$  ULTRACAM Sloan band colour would this binarity be true. We noticed at this point that the comparison star (TYC 6821-1317-1) has also a similar composite colour (blue in *Tycho-2*  $B - V$ , much redder in the other bands).

The extinction in the different spectral bands has been estimated. The stars are in the direction of the Galactic centre (inner Galaxy), above the plane ( $l = 352.4$  and  $b = 9.5$ ) which is at first sight a direction likely to be obscured by extinction if the star is not nearby. However, extinction models, such as Arenou, Grenon & Gómez (1992) and Marshall et al. (2006), predict a not so high absorption ( $A_{K_s} < 0.1$  mag corresponding to  $A_V < 0.9$ ) in this area, up to the distance of the galactic centre at least. From this result, we assumed that the absorption cannot be very high and we limited our search within the range of  $0 < A_V < 1.5$ . The adopted procedure was to use synthetic Sloan and 2MASS photometry plus extinction ratio in all these various bands to check against each spectral type/luminosity class and extinction, searching for the minimum distance between the observed and theoretical (unreddened+extinction) colours. We obtain that the most likely star type is an F0V with a  $A_V \sim 0.8$  mag absorption at 430 pc. This finally leads to a projected radius of 590 m at 50 au. Similar analysis was done for others target stars (Table 1). The four target stars have a projected size at 50 au smaller than 0.5 Fresnel scale.

## 3 EXPECTED OCCULTATION RATE

We used the data described above to calculate which objects are detectable with such observations. This in turn will allow us to

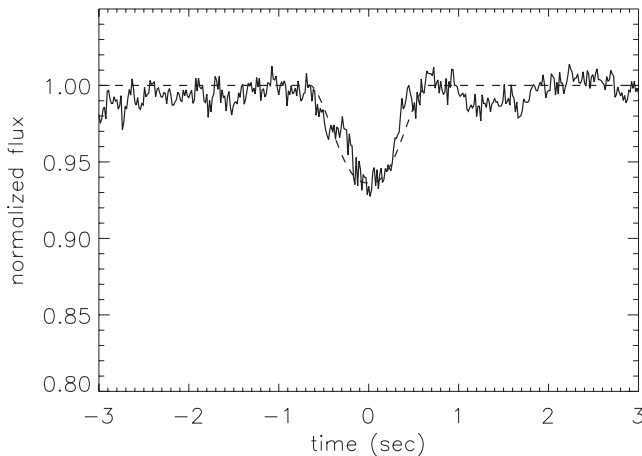
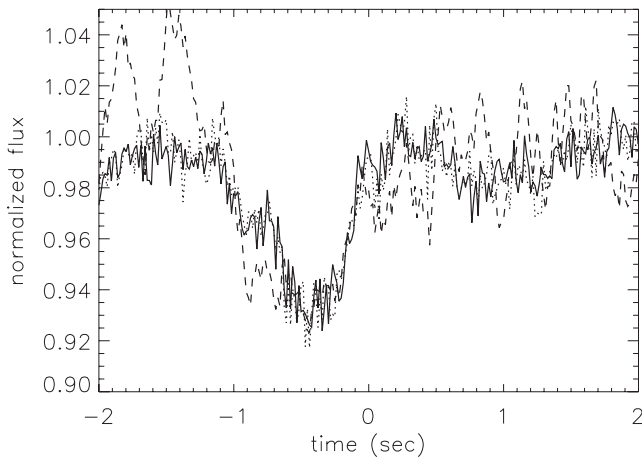
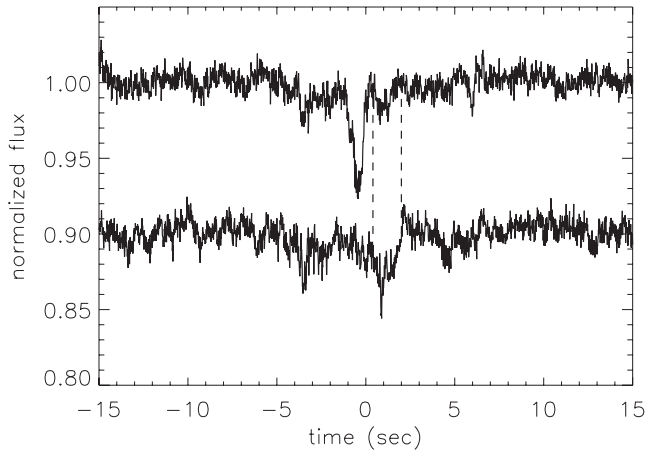


**Figure 3.** Potential event. (top) Normalized flux (sum of the three channels) of the star 1 (up) and the star 2 (down). (middle) Normalized fluxes in the three bands,  $g'$  (solid line),  $r'$  (dotted line) and  $u'$  (dashed line). (bottom) The synthetic profile of an occultation by a 4-km object at 1300 au with impact parameter = 0.75 times star radius is overlaid on the potential event light curve.

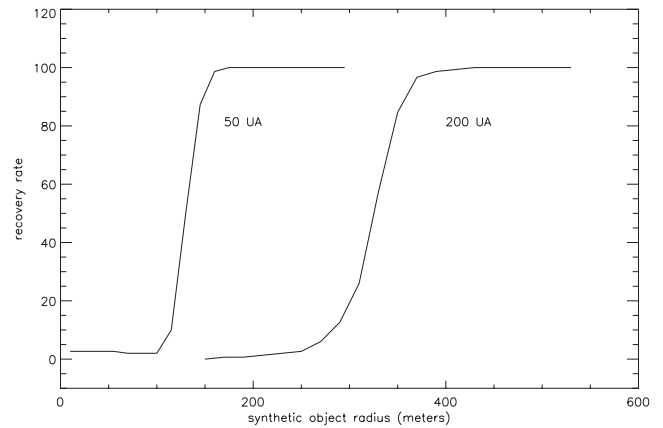


**Figure 4.** Recovery rate of synthetic event (at 50 and 200 au) implanted in our data set. The simulation shows that 100 per cent of the objects are found.

assess the instrumental approach to search for occultation events by TNOs.

### 3.1 Size of detectable object at 50 au

We investigate the minimum size of object detectable in our data. For this, we implanted synthetic events in the data and search for them. For each value of the object size, we computed synthetic profiles from the formula B5–B6 of Roques, Moncuquet & Sicardy (1987). The profile is smoothed on the wavelength interval and on the star surface considering a 0.015 mas radius star. We implant 150 profiles in the star 1 and in star 2 light curves. The search criterion is  $\Delta VI_{\text{int}} \geq 0.01$ . We found that, for objects at 50 au, the detection threshold is steep, no object smaller than 120 m radius is detected and 100 per cent of the objects larger than 150 m radius are found (Fig. 4).

### 3.2 Detectable object at 200 au

For synthetic profiles of objects orbiting at 200 au, few 250 m radius objects are detected and 90 per cent of the objects of 360 m radius. 100 per cent of objects of 420 m radius are detected.

### 3.3 Detectable object at 5000 au

A recovery rate of 90 per cent is obtained for 11 km radius objects and a rate of 100 per cent is obtained for a 15 km radius objects (Fig. 5) when the star size is  $1.4 \times 10^{-2}$  mas. If the star size is 10 times smaller, i.e. a  $1.4 \times 10^{-3}$  mas, a 2000 m radius comet at 5000 au is recovered with a 100 per cent rate (Fig. 5).

### 3.4 Expected occultation rate

The above analysis shows that light curves obtained with a 8-m telescope allow us to detect TNO of 150 m radius. This is in good agreement with the Bickerton et al. (2008) analysis. The published detection of a 500 m TNO in *HST* data by Schlichting et al. (2009) allows us to make two hypothesis on the density of TNO of 150 m radius in the sky plane: for this, we consider a cumulative size distribution of TNO with two values of the slope of  $q = 3.9$  and  $3.5$  for the small TNO cumulative size distribution and a normalization of  $N(>r) = 5.4$  objects per square degree for a radius of 45 km (Fuentes et al. 2009). The slope of 3.9 is the best estimate from the

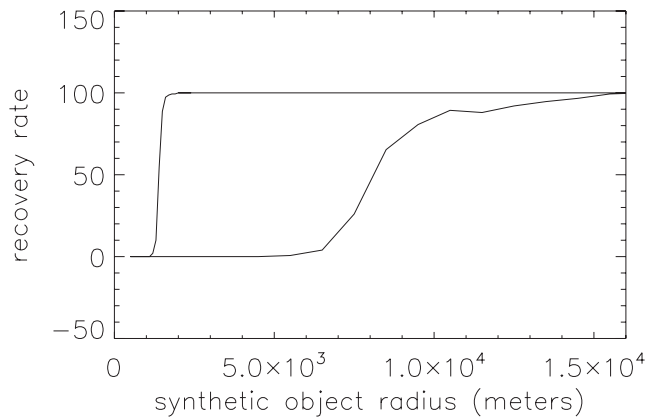


**Figure 5.** Recovery rate of synthetic event (at 5000 au) implanted in the data set. Right curve: the synthetic profile is computed with a  $1.4 \times 10^{-2}$  mas radius star. Left curve: the synthetic profile is computed with a  $1.4 \times 10^{-3}$  mas radius star.

detection of the *HST* event (Schlichting et al. 2009), and a slope of 3.5 corresponds to collisional cascade of strength-dominated bodies. This leads to two values for the average time between occultations of one star by 150 m radius TNO: one value of five nights for a slope of 3.9 and 50 nights for a slope of 3.5. This expected occultation rate is too small to allow an exploration of the Kuiper belt with observation of only 1 or 2 stars simultaneously, taking into account the difficulty of obtaining large telescope observing time. As a VLT is mandatory, we have to monitor simultaneously several stars to detect enough events for a reliable statistical analysis.

### 3.5 Number of target stars

Let us estimate the number of suitable target stars we can expect. According to Roques & Moncuquet (2000), stars with a projected size smaller than 0.5 Fresnel scale give well-defined diffracting profile (provided that time sampling and S/N are high enough). To estimate the number of target stars, let us fix an acquisition rate of 50 Hz. This provides 10 points for the diffracting profile of a 0.2-s event (time duration in the configuration of the above observation).

We consider stars which magnitude is smaller than 13.5 (to get an S/N larger than 100 at 50 Hz). For stars of the main sequence, and without taking into account interstellar extinction and reddening, half of the  $m < 13.5$  stars have a size projected at 50 au smaller than half the Fresnel scale at this distance. This gives hundredths of stars per square degree well adapted for search of hectometre TNO by serendipitous stellar occultations with a 8-m telescope. For example, in the field of view of the Nasmyth focus of the VLT, which has a 25 arcmin diameter, 50–100 well-adapted target stars could be chosen (Fig. 6).

## 4 THE INSTRUMENTAL CONCEPT

### 4.1 Fast multi-object photometry

The previous section shows that there are fields with 50–100 stars well adapted for the detection of hectometre-sized TNO by stellar occultations. The simultaneous record of these stars needs the possibility of monitoring several targets in a large field with frequency higher than 50 Hz with no dead time. This is not possible with large CCD whose readout time is too large. The instrumental concept of Multi-Object instrument used bun-

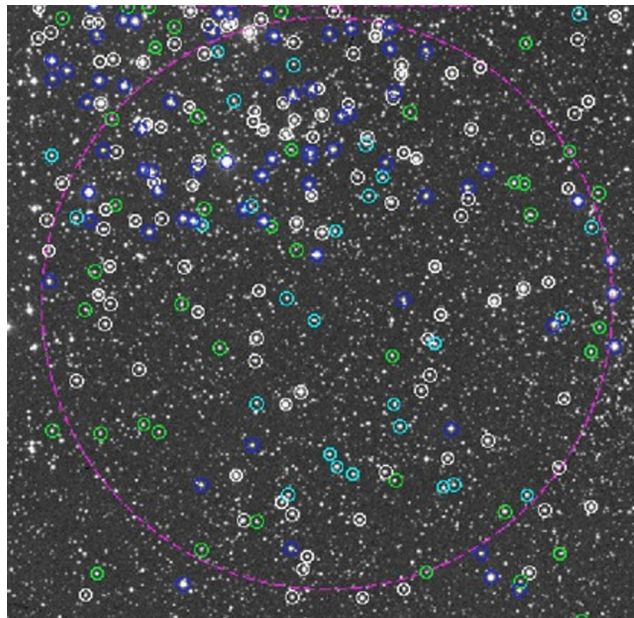


**Figure 6.** Field of view of the Nasmyth focus of the VLT, which has a 25 arcmin diameter. Circled coloured stars are selected targets with magnitude brighter than 12.5.

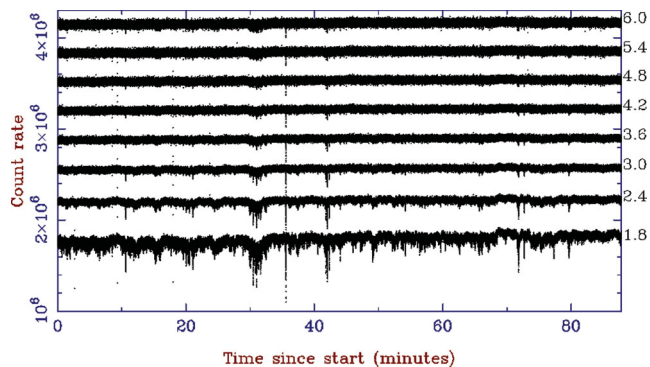


**Figure 7.** Simulated light-curve fibre bundles of different sizes. The curves are computed with fixed aperture from 67 Hz ULTRACAM images. The aperture diameters in arcsec are given on the right-hand side of the image.

dle of fibres to record simultaneously several targets on a large field, as the ESO instrument FLAMES mounted on the VLT (<http://www.eso.org/sci/facilities/paranal/instruments/flames/>). A similar concept of fibre multi-object photometer allows monitoring simultaneously several targets in a large field.

A critical issue is the aperture of a single fibre. The angular size should be large enough to avoid false events due to stellar flux loss because of scintillation. Tests have been done with the ULTRACAM images to simulate light curves obtained with a constant aperture. These tests show that a 4 arcsec diameter aperture allows us to eliminate most of the scintillation fluctuation (Fig. 7). This result depends on the observation conditions and an instrument based on this concept will need to study carefully this parameter. However, these tests show that a 4 arcsec field of view would be sufficient for our purpose. Such a field of view cannot be obtained with a single fibre; however, a bundle of several ( $3 \times 3$ ) fibres could achieve this goal.

A set of fibre bundles feeding a CCD could be a Fast Multi-Object Photometer (F-MOP) allowing us to record simultaneously a large number of stars at high acquisition frequency.

#### 4.2 Performance of an F-MOP for the exploration of the outer Solar system

We have shown above that an F-MOP mounted on a 8 m class telescope can detect 150 m radius TNO with a recovery rate of 100 per cent. The time between occultations by such TNOs can be estimated to be 5–50 nights for a given star. This estimation supposes that the F-MOP has the same instrumental performance as ULTRACAM. Such an F-MOP with 100 fibre bundles would detect between 2 and 20 TNO occultation profiles per night.

The limit of such instrument is the possible detection of false positive events due to atmospheric artefacts. As shown in Section 2.3, atmospheric fluctuations can mimic an occultation profile of a large star, i.e. without diffraction fringes. The frequency of such atmospheric fluctuations cannot be estimated from the data set used here, but they are very rare (E. Gendron, private communication). Moreover, if the star is small enough, occultation profile by a TNO always has diffraction fringes which cannot be mimicked by an atmospheric fluctuation, provided that the observation frequency is large enough.

The exploration of the Oort cloud by stellar occultations is possible with an F-MOP mounted on a 8-m telescope. The star target must be very small but bright enough for the diffraction profile to be observable. Observations with similar S/N as our data set would need two orders of magnitude longer duration to detect Oort cloud objects. This can be achieved from ground with multi-object fast photometry on large telescopes large enough to provide high S/N.

## 5 CONCLUSIONS

Observations with the fast camera ULTRACAM on the VLT have been used to explore the possibility of exploration of the outer Solar system with a multi-object photometer and a VLT. These results show that fast ( $>60$  Hz) photometric observations with  $S/N \geq 100$  are able to exploit the occultation method for the exploration of the trans-Neptunian region (Roques et al. 2008). The detection of large number of occultation events would allow discriminating between various models of the Kuiper belt. Oort cloud objects could be detected with such an approach. The selection of small angular targets stars and multiwavelength information are necessary to discriminate occultation events from atmospheric noise in the light curves.

## ACKNOWLEDGMENTS

We thank the Programme National de Planétologie (PNP) and the Agence National pour la Recherche (grant ANR BLAN08-2\_328288 Beyond Neptune) for financial support of this research.

The VLT-ULTRACAM light curves are available on the website: <http://lesia.obspm.fr/beyond-neptune/ultraphot/data-archive/> for the purpose of tests on detection methods.

## REFERENCES

- Arenou F., Grenon M., Gómez A., 1992, *ApJ*, 258, 104  
 Bernstein G. M., Trilling D. E., Allen R. L., Brown M. E., Holman M., Malhotra R., 2004, *AJ*, 128, 1364  
 Bianco F. B., Protopapas P., McLeod B. A., Alcock C. R., Holman M. J., Lehner M. J., 2009, *AJ*, 138, 568  
 Bickerton S. J., Kavelaars J. J., Welch D. L., 2008, *AJ*, 135, 1039  
 Dhillon V. S. et al., 2007, *MNRAS*, 378, 825  
 Epchtein N. et al., 1997, *The Messenger*, 87, 27  
 Farinella P., Davis D. R., Stern S. A., 2000, in Mannings V., Boss A. P., Russell S. S., eds, *Protostars and Planets IV*. Univ. Arizona Press, Tucson, p. 1255  
 Fraser W. C. et al., 2008, *Icarus*, 195, 827  
 Fuentes C. I., George M. R., Holman M. J., 2009, *AJ*, 696, 91  
 Fukugita M., Ichikawa T., Gunn J. E., Doi M., Shimasaku K., Schneider D. P., 1996, *AJ*, 111, 1748  
 Høg E. et al., 2000, *A&A*, 355, L27  
 Kenyon S. J., Luu J. X., 1998, *AJ*, 115, 2136  
 Malhotra R., Duncan M. J., Levison H. F., 2000, in Mannings V., Boss A. P., Russell S. S., eds, *Protostars and Planets IV*. Univ. Arizona press, Tucson, p. 1231  
 Marshall D., Robin A. C., Reylé C., Schultheis M., Picaud S., 2006, *A&A*, 453, 635  
 Morbidelli A., Levison H. F., Gomez R., 2008, in Barucci M. A., Boehnhardt H., Cruikshank D. P., Morbidelli A., eds, *The Solar System Beyond Neptune*. Univ. Arizona press, Tucson, p. 275  
 Nihei T. C., Lehner M. J., Bianco F. B., King S.-K., Giammarco J. M., Alcock C., 2007, *AJ*, 134, 1596  
 Petit J.-M., Kavelaars J.-J., Gladman B., Loredó T., 2008, in Barucci M. A., Boehnhardt H., Cruikshank D. P., Morbidelli A., eds, *The Solar System Beyond Neptunem*. Univ. Arizona press, Tucson, p. 275  
 Roques F., Moncuquet M., 2000, *Icarus*, 147, 530  
 Roques F., Moncuquet M., Sicardy B., 1987, *AJ*, 93, 1549  
 Roques F., Moncuquet M., Lavillonière N., Auvergne M., Chevreton M., Colas F., Lecacheux J., 2003, *ApJ*, 594, L63  
 Roques F. et al., 2006, *AJ*, 132, 819 (R06)  
 Roques F., Georgesvits G., Doressoundiram A., 2008, in Barucci M. A., Boehnhardt H., Cruikshank D. P., Morbidelli A., eds, *The Solar System Beyond Neptune*, Univ. Arizona press, Tucson, p. 545  
 Roques F., Guinouard I., Buey J.-T., Doressoundiram A., Horville D., Marteaud M., 2009, in Moorwood A., ed., *Astrophys. Space Sci. Proc., Science with the VLT in the ELT Era*. Springer, Dordrecht, p. 429  
 Schlichting H. E., Sari R., 2011, *ApJ*, 728, 68  
 Schlichting H. E., Ofek E. O., Wenz M., Sari R., Gal-Yam A., Livio M., Nelan E., Zucker S., 2009, *Nat*, 462, 895  
 Skrutskie M. F. et al., 2006, *AJ*, 131, 1163  
 Trujillo C. A., Jewitt D. C., Luu J. X., 2001, *AJ*, 122, 457

This paper has been typeset from a  $\text{\TeX}/\text{\LaTeX}$  file prepared by the author.